X-Ray Emission from M32: X-Ray Binaries or a μAGN?

Paul B. Eskridge, Raymond E. White III, and David S. Davis
Department of Physics and Astronomy, University of Alabama, Tuscaloosa, AL 35487

ABSTRACT

We have analysed archival *ROSAT* PSPC data for M32 in order to study the x-ray emission from this nearest elliptical galaxy. We fit spectra from three long exposures with Raymond-Smith, thermal bremsstrahlung, and power-law models. All models give excellent fits. The thermal fits have kT≈4 keV, the Raymond-Smith iron abundance is $0.4^{+0.7}_{-0.3}$ Solar, the power-law fit has α=1.6±0.1, and all fits have N_H consistent with the Galactic column. The source is centered on M32 to an accuracy of 9″, and unresolved at 27″ FWHM (∼90 pc). M32 is x-ray variable by a factor of 3–5 on timescales of a decade down to minutes, with evidence for a possible period of ∼1.3 days.

There are two plausible interpretations for these results: 1) Emission due to low-mass x-ray binaries; 2) Emission due to accretion onto a massive central black hole. Both of these possibilities are supported by arguments based on previous studies of M32 and other old stellar systems; the *ROSAT* PSPC data do not allow us to unambiguously choose between them. Observations with the *ROSAT* HRI and with *ASCA* are required to determine which of these two very different physical models is correct.

Subject headings: galaxies: active – galaxies: elliptical and lenticular, cD – galaxies: individual: M32 – X-rays: galaxies

1. Introduction

M32 (NGC 221, PCG 2555) is not only the nearest (D≈700 kpc, e.g. Ciardullo et al. 1989) example of the low-luminosity end of the sequence of normal elliptical galaxies (Kormendy 1985), but the nearest such elliptical of any luminosity. This allows us to study it to much lower absolute luminosity and size limits than is possible for other more luminous ellipticals. The Virgo cluster is ∼20 times more distant than M32 (e.g. Pierce et al. 1994), thus observations at a given angular scale or flux limit probe ∼400 times deeper for M32 than for Virgo Es. As a result, our understanding of the properties of M32 provides us with a cornerstone for the investigation of more luminous and more distant ellipticals.

X-ray emission from faint early-type galaxies ($L_B \lesssim 10^{40}$ erg s^{-1}) typically has a hard ($\sim$5 keV) spectrum, with $L_X \propto L_B$ (Kim, Fabbiano & Trinchieri 1992a; Eskridge, Fabbiano & Kim 1995). This emission is interpreted as arising from population II stellar binary sources (low mass x-ray binaries, or LMXRBs). The *Einstein* data for M32 are consistent with this interpretation (e.g. Fabbiano, Kim & Trinchieri 1992), however the *Einstein* observation of M32 was not particularly deep; other models for the x-ray emission are not excluded. In particular, optical imaging and spectroscopy both indicate that M32 contains a central black hole of $M_\bullet \approx 1$–$3\times10^6 M_\odot$ (van der Marel et al. 1994; Lauer et al. 1992). The observed x-ray emission may be due to low-level accretion onto this black hole.

We have analysed archival *ROSAT* PSPC observations of M32 in order to study the nature of the x-ray emission with the best currently available data. In §2 we discuss the available PSPC data. In §3 we investigate the spectral properties, extendedness, and time variability of the x-ray emission. We discuss the two possible physical interpretations of these data in §4, and conclude with a discussion of crucial future observations in §5.

2. PSPC Observations

There are many pointings that include M32 in the *ROSAT* Public Archive. Most are short ($\sim$2–3 ksec), but there are three long unobstructed pointings ($\gtrsim$28 ksec), details of which are given in Table 1. The total integration time from these pointings is $\sim$101 ksec. We use these data for spectral analysis in §3.1 below. We use two pointings to analyse the source extent in §3.2: WP600363N00 is the pointing nearest to on-axis but is only a $\sim$2 ksec exposure; WP600068 (17′ off-axis) is the long pointing nearest to on-axis. We use the short pointings to search for source variability in §3.3 below.

3. Analysis

3.1. Spectral Properties

We fit the vignetting-corrected data from the three long pointings to spectral models using *XSPEC v9.0*. The source count-rate is $\sim$0.1s^{-1}. Source spectra were extracted from circular regions centered on M32, with radii of 2.′3–5.′2 (or 3.8–8.7R_e for $R_e = 0.'6$, de Vaucouleurs et al. 1991) depending on the off-axis distance of M32 in each pointing. We adopted a maximum master-veto rate of 170. Background regions were chosen from adjacent source-free areas. Errors were calculated using Poisson statistics, with systematic errors of 1% included in quadrature. We fit three kinds of spectral models to the data:

Raymond-Smith (RS) thermal models, thermal bremsstrahlung (TB), and power-law (PL) models. These models incorporate an absorption component with Morrison & McCammon (1983) cross-sections. As M32 exhibits significant variability (see §3.3 below), the normalizations for each pointing were allowed to vary independently.

All three spectral models provide formally excellent fits to the data, with the RS model being the best by a small margin (see Table 2). The best-fit RS model has kT≈3.9 keV, and an abundance of ∼0.4 Solar (with large error bounds). The best-fit TB model has kT≈4.3 keV. The best-fit PL model has a photon index of $\alpha \approx 1.6$. The best-fit RS model is shown with the three data sets (with different normalizations) in Figure 1a,b. The best-fits to the data for the three spectral models are essentially indistinguishable. The fit N_H is consistent with the observed Galactic column ($N_H \approx 6.6 \times 10^{-20}$ cm^{-2} Stark et al. 1992) for all models. The TB model has a higher χ^2 than the RS model: $\Delta\chi^2 = +5.8$ for $\Delta\nu = +1$. The F-test (which tests if the reduction in χ^2 due to an additional fitted parameter is significant) suggests that the line-producing RS model is preferred to the zero-abundance TB model at the ∼98% level. The fluxes and luminosities implied by these spectral models are given in Table 3 for both *ROSAT* and *Einstein* energy bands. The fluxes from the three pointings differ by ∼10%, an amount much larger than the change in flux between different models for a given pointing. We believe this is due to the intrinsic variability of the source (discussed in §3.3, below).

We searched for evidence of emission from gas at or near the kinetic temperature of the stars (40≤kT≤200 for a central velocity dispersion of 77 km s^{-1}, McElroy 1995), but found that the flux attributable to any such cool component is $\lesssim$1% of the total.

3.2. Extendedness

The on-axis exposures are all $\lesssim$3 ksec, and thus do not provide good counting statistics for evaluating the extendedness of M32. Therefore, we use both WP600363N00, a ∼2 ksec exposure with M32 3′ off-axis, and WP600068, a 30.6 ksec exposure with M32 17′ off-axis. The central region of WP600068 is displayed in Figure 2a. We used *PROS* to produce this image from the initial data file, and *ftools v3.3* to generate the exposure map. Figure 2b is a contour-plot of M32, and shows an extension to the NE due to a second, partially resolved faint source (with a count-rate $\lesssim$4% that of the main source). The nature of this second source is unclear. We fit the radial profile of M32 in WP600068 (excluding $0° \leq PA \leq 90°$ in order to avoid the second source) with a PSF appropriate for a 17′ off-axis PSPC observation (Hasinger et al. 1995). This PSF has a FWHM≈46″.3 ($1.3R_e$ or ∼160 pc). The profile is well-fit by the PSF (see Figure 3). A similar analysis of WP600363N00

indicates that M32 is unresolved at 27″ FWHM (∼0.75 R_e, or ∼90 pc), although with much poorer counting statistics. We measured the position of the M32 x-ray source in the image WP600342. Using the point-sources 5C 03.076 and M31 40 1650[1] to transform the astrometry, we derive an x-ray position for M32 of $00^h42^m41\overset{s}{.}7$, $+40°51'45\overset{''}{.}1$ (J2000). This differs from the RC3 optical position by ∼9″, comparable to the PSPC positional accuracy.

3.3. Time Variability

For a 4 keV TB model the average flux from the PSPC implies a flux in the *Einstein* band that is ∼3 times that observed in 1980 (the other spectral models give the same result – see Table 3). Thus M32 is x-ray variable on the timescale of a decade. In Figure 4a, we show the count-rate time series for all PSPC pointings with M32 ≤40′ off-axis. These data are sparsely sampled, but show clear variability with an amplitude of ∼1 dex on timescales of months to a year. Fig. 4b shows the best-sampled part of the time series. We fit these data with a phase dispersion minimization algorithm, and find evidence for a period of 1.27 days. A second moderately well-sampled part of the time series, around day 540, shows evidence for a similar period (1.37 days), but this is based on only twelve data points. We attempted to phase these two samples together, searching for a period in the range 1.1–1.5 days. None was found. Thus the available data show no sign of a coherant binary period over a gap of ∼200 days, arguing that the evidence for periodicity in the short samples may be spurious. We also studied the count-rate data for the pointing WP600068 to search for shorter timescale variability. We note that although M32 is near the PSPC ring structure in this exposure, it is *not* close enough to be significantly effected by the spacecraft wobble. While both the Kolmogorov-Smirnov and the Cramer-von Mises tests argue that the source is variable (at the >99% and 95% levels, repectively), we find no convincing period aside from the orbital period (∼90 min).

4. Discussion

The x-ray data for M32 suggest two possible interpretations: 1) The x-rays are due to the integrated emission from a population of LMXRBs. 2) The x-rays are due to emission from accretion onto a massive central black hole. Below, we review the available evidence for and against each of these interpretations.

---

[1]This star is just west of NGC 206. Its optical and x-ray luminosities are consistent with it being a high-mass x-ray binary in the disk of M31.

4.1. The Case for LMXRBs

The L_X for M32 corresponds to the Eddington luminosity (L_E) for a 1–3$M_\odot$ object, and is in keeping with the L_X–L_B relationship for x-ray faint early-type galaxies (Eskridge et al. 1995). The standard interpretation for x-ray emission from such galaxies is that it is due to LMXRBs (e.g. Kim, Fabbiano & Trinchieri 1992b). There is an extensive literature on the stellar populations of M32 (e.g. Buzzoni 1995, and references therein). Although many studies indicate a significant intermediate age population exists (references in Buzzoni 1995), the dominant population in terms of mass appears to be old. Thus one would expect a population of LMXRBs. The best-fit thermal model to the *ROSAT* spectrum has kT$\sim$4 keV, consistent with results for Galactic LMXRBs (e.g. White, Nagase & Parmar 1995). The RS abundance is $0.1 \leq Z_\odot \leq 1.2$. Estimates from integrated nuclear spectroscopy are in the range $-0.5 \leq [Fe/H] \leq -0.1$ (0.3 — 0.8 $Z_\odot$) (e.g. Hardy et al. 1994 and references therein). The x-ray result thus agrees with the optical results. We noted above that M32 is x-ray variable on timescales from a decade down to a day. Galactic LMXRBs are x-ray variable on $\sim$day timescales due to the binary periods, and exhibit x-ray flaring and quasi-periodic behaviour on longer timescales (e.g. White et al. 1995). The number of LMXRBs needed to account for the observed x-ray flux from M32 is small, only 1–5 objects, thus the observed global variability is consistent with the LMXRB interpretation.

4.2. The Case for a μAGN

The *ROSAT* data are as well fit by an α=1.6$\pm$0.1 PL model as by a thermal model. An α=1.7 PL is the canonical x-ray spectrum for AGN (e.g. Mushotzky, Done & Pounds 1993). AGN are well known to be x-ray variable (e.g. Mushotzky et al. 1993) on the timescales and with the amplitudes observed. There is no evidence that the main source is extended at the level of $0.75R_e$. We are thus forced to take seriously the possibility that the x-ray emission from M32 is due to a μAGN.

The possible existence of a massive central black hole in M32 has been discussed for the last dozen years (e.g. van der Marel et al. 1994 and references therein). The relevant data are the nuclear rotation and velocity dispersion profiles, and the nuclear luminosity profile. Van der Marel et al. (1994) analyse high spatial and spectral resolution, high S/N nuclear spectra of M32. They conclude that their data can be explained by the presence of a central black hole of $M_\bullet \approx 1.8 \times 10^6 M_\odot$. Imaging of the central luminosity cusp at a resolution of $0\farcs04$ by Lauer et al. (1992) supports the existence of a central black hole of $M_\bullet \approx 3 \times 10^6 M_\odot$. These studies also strongly constrain non-black hole models, in that the relaxation and stellar collision timescales for extended mass distributions that can produce

their results are $\sim 10^{-2}$ of a Hubble time.

The L_E for a black hole of $M_\bullet \approx 3 \times 10^6 M_\odot$ is $\sim 4 \times 10^{44}$ erg s^{-1}, six dex higher than the observed L_X. The low L_X can be attributed to a lack of fuel for the central engine: $M_{HI} < 5 \times 10^5 M_\odot$ (Roberts et al. 1991); $L_{FIR} < 3 \times 10^{36}$ erg s^{-1} (Knapp et al. 1989). This is also reflected in the lack of any other observational signals of an AGN: $P_{6cm} \leq 1$ mJy (Roberts et al. 1991); the limit to the equivalent width of Hα is <6Å in a 3″ aperture (Kennicutt & Kent 1983), or ≤ 1.8Å in a 1″ aperture (Keel 1983). This implies $f_{H\alpha} \lesssim 10^{-15}$ erg cm^{-2} s^{-1} (W. Keel, private communication). The $f_{H\alpha}/f_X$ ratio is moderately lower than in typical AGN (e.g. Blumenthal, Keel & Miller 1982; Mulchaey et al. 1994), but not strikingly so. If we take the observed $L_X \approx 10^{38}$ erg s^{-1} as the bolometric luminosity of the central engine, we can use the well known relationship,

$$\dot{M} \approx \frac{2L}{c^2}, \tag{1}$$

to determine a mass accretion rate of 1–2$\times 10^{-9} M_\odot$ yr^{-1}. Such a fueling rate clearly offers no conflict with the low observational limits on AGN activity or ISM content in other wavebands. Finally, we note that if the x-rays *are* due to LMXRBs, then the putative central black hole is being fueled at a much lower rate than $10^{-9} M_\odot$ yr^{-1}.

5. Conclusion

We have presented arguments that the x-ray emission from M32 can be due to *either* a small population of LMXRBs, *or* accretion onto the massive central black hole. Two observations that could resolve this ambiguity are *ROSAT* HRI imaging and *ASCA* spectroscopy. A deep on-axis HRI image would determine the extent and position of the M32 x-ray source much more precisely than do the PSPC data. It would also resolve the weak source to the NE. The HRI on-axis PSF is $\sim 6''$ FWHM ($\sim 0.17 R_e$) giving a spatial resolution of $\sim$20 pc. Emission from an AGN would thus be unresolved with the HRI, and would come from the center of M32. Emission from a collection of LMXRBs would not have to be coincident with the center of M32, and could be extended at HRI resolution. A deep *ASCA* spectrum will have the spectral resolution to clearly distinguish between the thermal and power-law spectral models in an integration time of $\sim$20 ksec. Given the importance and proximity of M32, the opportunity to resolve the current puzzle should not be missed.

We thank Bill Keel for access to his unpublished nuclear spectrum of M32, and for useful discussions about AGN. We also thank Jeff McClintock and Andy Silber for advice on the properties of LMXRBs. This research has made use of the NASA/IPAC Extragalactic

Database (NED) which is operated by the Jet Propulsion Laboratory, Caltech, under contract with the National Aeronautics and Space Administration. This research was supported by the EPSCoR program under Grant No. EHR-9108761, and by the National Aeronautics and Space Administration under ROSAT Grants No. NAG 5-1973 and NAG 5-1718.

REFERENCES

Blumenthal, G.R., Keel, W.C., & Miller, J.S. 1982, ApJ, 257, 499.

Buzzoni, A. 1995, ApJS, 98, 69.

Ciardullo, R., Jacoby, G.H., Ford, H.C., & Neill, J.D. 1989, ApJ, 339, 53.

de Vaucouleurs, G., de Vaucouleurs A., Corwin, H.G., Jr., Buta, R.J., Paturel, G., & Fouqué, P. 1991, Third Reference Catalogue of Bright Galaxies (New York: Springer-Verlag).

Eskridge, P.B., Fabbiano, G., & Kim, D.-W. 1995, ApJS, 97, 141.

Fabbiano, G., Kim, D.-W., & Trinchieri, G. 1992, ApJS, 80, 531.

Hardy, E., Couture, J., Couture, C., & Joncas, G. 1994, AJ, 107, 195.

Hasinger, G., Boese, G., Predehl, P., Turner, T.J., Yusaf, R., George, I.M., & Rohrbach, G. 1995, MPE/OGIP Calibration Memo CAL/ROS/93-015.

Keel, W.C. 1983, ApJ, 269, 466.

Kennicutt, R.C., & Kent, S.M. 1983, AJ, 88, 1094.

Kim, D.-W., Fabbiano, G., & Trinchieri, G. 1992a, ApJS, 80, 645.

Kim, D.-W., Fabbiano, G., & Trinchieri, G. 1992b, ApJ, 393, 134.

Knapp, G.R., Guhathakurta, P., Kim, D.-W., & Jura, M. 1989, ApJS, 70, 329.

Kormendy, J. 1985, ApJ, 295, 73.

Lauer, T.R., et al. 1992, AJ, 104, 552.

McElroy D.B. 1995, ApJS, 100, 105.

Morrison, R., & McCammon, D. 1983, ApJ, 270, 119.

Mulchaey, J.S., Koratkar, A., Ward, M.J., Wilson, A.S., Whittle, M., Antonucci, R.R.J., Kinney, A.L., & Hurt, T. 1994, ApJ, 436, 586.

Mushotzky, R.F., Done, C., & Pounds, K.A. 1993 ARA&A, 31, 717.

Pierce, M.J., Welch, D.L., McClure, R.D., van den Bergh, S., Racine, R., & Stetson, P.B. 1994, Nature, 371, 385.

Roberts, M.S., Hogg, D.E., Bregman, J.N., Forman, W.R., & Jones, C. 1991, ApJS, 75, 751.

Stark, A.A., Gammie, C.F., Wilson, R.W., Bally, J., Linke, R.A., Heiles, C., & Hurwitz, M. 1992, ApJS, 79, 77.

van der Marel, R.P., Wyn Evans, N., Rix, H.-W., White, S.D.M., & de Zeeuw, T. 1994, MNRAS, 271, 99.

White, N.E., Nagase, F., & Parmar, A.N. 1995, in X-Ray Binaries, ed. W.H.G. Lewin, J. van Paradijs & E.P.J. van den Heuvel (Cambridge: Cambridge U. Press), 1.

Table 1 – Long *ROSAT* PSPC Pointings Including M32

Seq. ID	Exp. time sec	RA(J2000) h m s	Dec(J2000) $\circ$ $\prime$ $\prime\prime$	Offset Angle
WP600068	30594	00 42 28	41 08 24	$17'$
WP600067	27970	00 43 55	41 30 36	$41'$
WP600079	42164	00 39 36	40 24 00	$45'$
Total integration	100728			

Table 2 - Model Fitting Results

Model	kT keV	range[1]	Z $Z_\odot$=1	range[1]	α	range[1]	N_H 10^{-20} cm^{-2}	range[1]	χ^2/ν
R-S	3.94	2.88–5.67	0.44	0.13–1.16			7.18	6.31– 8.34	89.5/104=0.86
Bremm.	4.25	3.07–6.01					7.71	6.81– 9.05	95.3/105=0.91
Power-law					1.57	1.46–1.71	8.45	7.29–10.23	102.0/105=0.97

1. The ranges given are the 90% confidence-limits.

Table 3 - Derived Fluxes and Luminosities

Model	Pointing	Flux[1] 0.2–2.0 keV	Luminosity[2] 0.2–2.0 keV	Flux[1] 0.5–4.0 keV	Luminosity[2] 0.5–4.0 keV
Raymond-Smith	WP600079	1.92	1.13	3.24	1.90
	WP600067	1.85	1.08	3.13	1.84
	WP600068	1.61	0.94	2.72	1.60
Bremmstrahlung	WP600079	1.95	1.14	3.36	1.97
	WP600067	1.88	1.10	3.24	1.90
	WP600068	1.64	0.96	2.83	1.66
Power-Law	WP600067	1.97	1.16	3.67	2.15
	WP600067	1.90	1.11	3.53	2.07
	WP600068	1.65	0.97	3.08	1.81

1. Flux in units of 10^{-12} erg s^{-1} cm^{-2}

2. Luminosity in units of 10^{38} erg s^{-1} for an assumed distance of 700 kpc.

Fig. 1.— The *ROSAT* PSPC spectra for M32 from three long pointings. a) Data from the three pointings with the best-fitting RS model. The data from WP600068 have the highest amplitude, those from WP600067 have the lowest. b) χ^2 as a function of energy for the RS fit.

Fig. 2.— a) The central $50' \times 50'$ of *ROSAT* image WP600068. North is up, East to the left. The image center is at $\alpha = 00^h42^m28\overset{s}{.}7$, $\delta = +41°08'24''$ (J2000). The complex emission at ($-150''$,$490''$) is the central area of M31. M32 is $\sim 17'$ off-axis to the south. b) A contour-plot of the $6\overset{'}{.}25 \times 6\overset{'}{.}25$ region centered on M32. The low contour is at 6 counts per pixel (a significance level of 2.3σ), with subsequent contours at factor of 2 intervals . Note the obvious extension to the NE caused by a second, much fainter source.

Fig. 3.— The radial profile of M32 from *ROSAT* image WP600068 with the range $0° \leq PA \leq 90°$ excluded. The solid line is the PSF for a source $17'$ off-axis.

Fig. 4.— The PSPC light-curve for M32. a) All data from pointings $\leq 40'$ off-axis. b) The moderately well sampled part of the light curve around UTC 388. These data show evidence for a periodicity of $\sim$1.27 days.

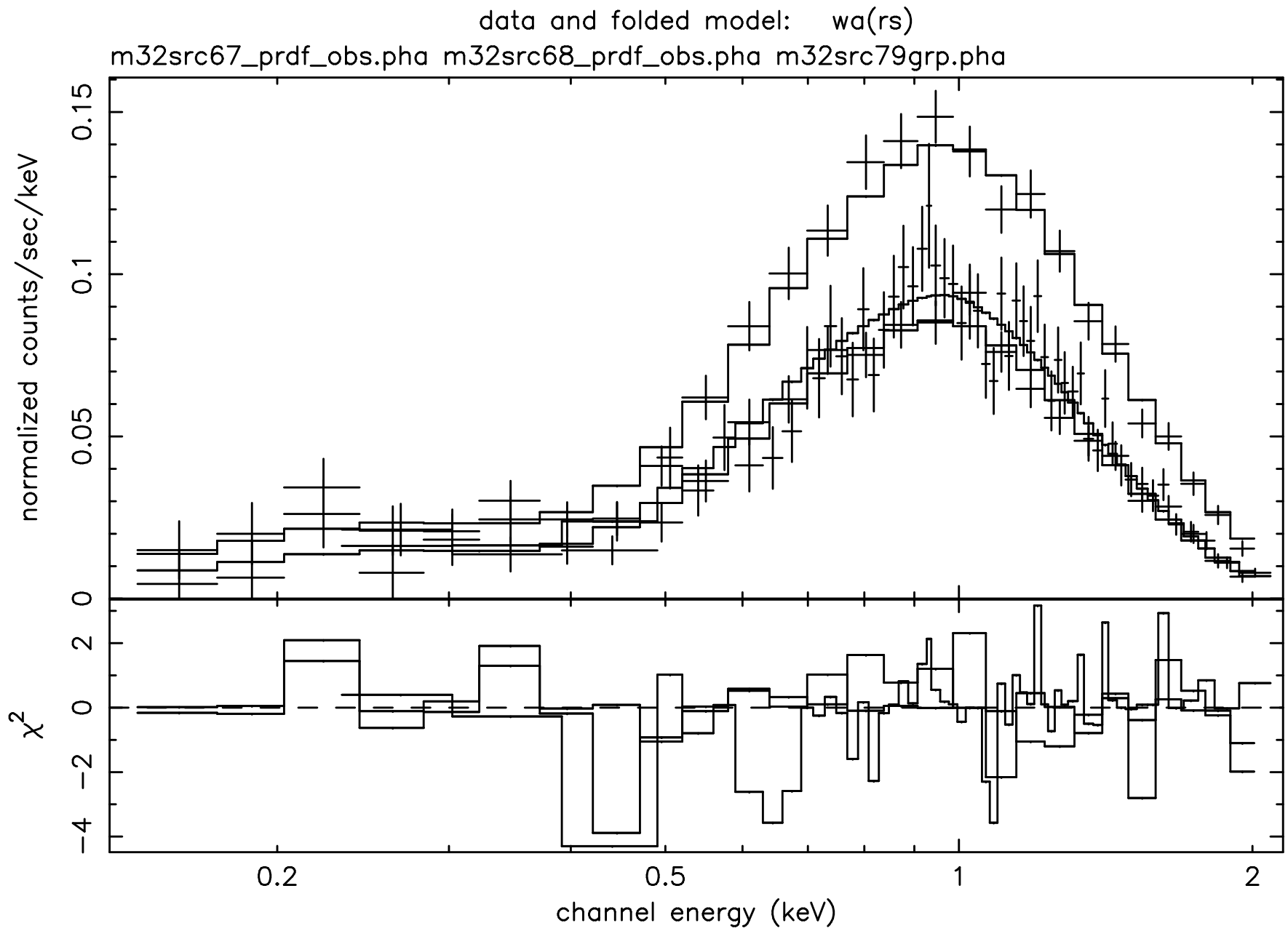

white 19−Dec−1995 20:55

M32 Figure 2a

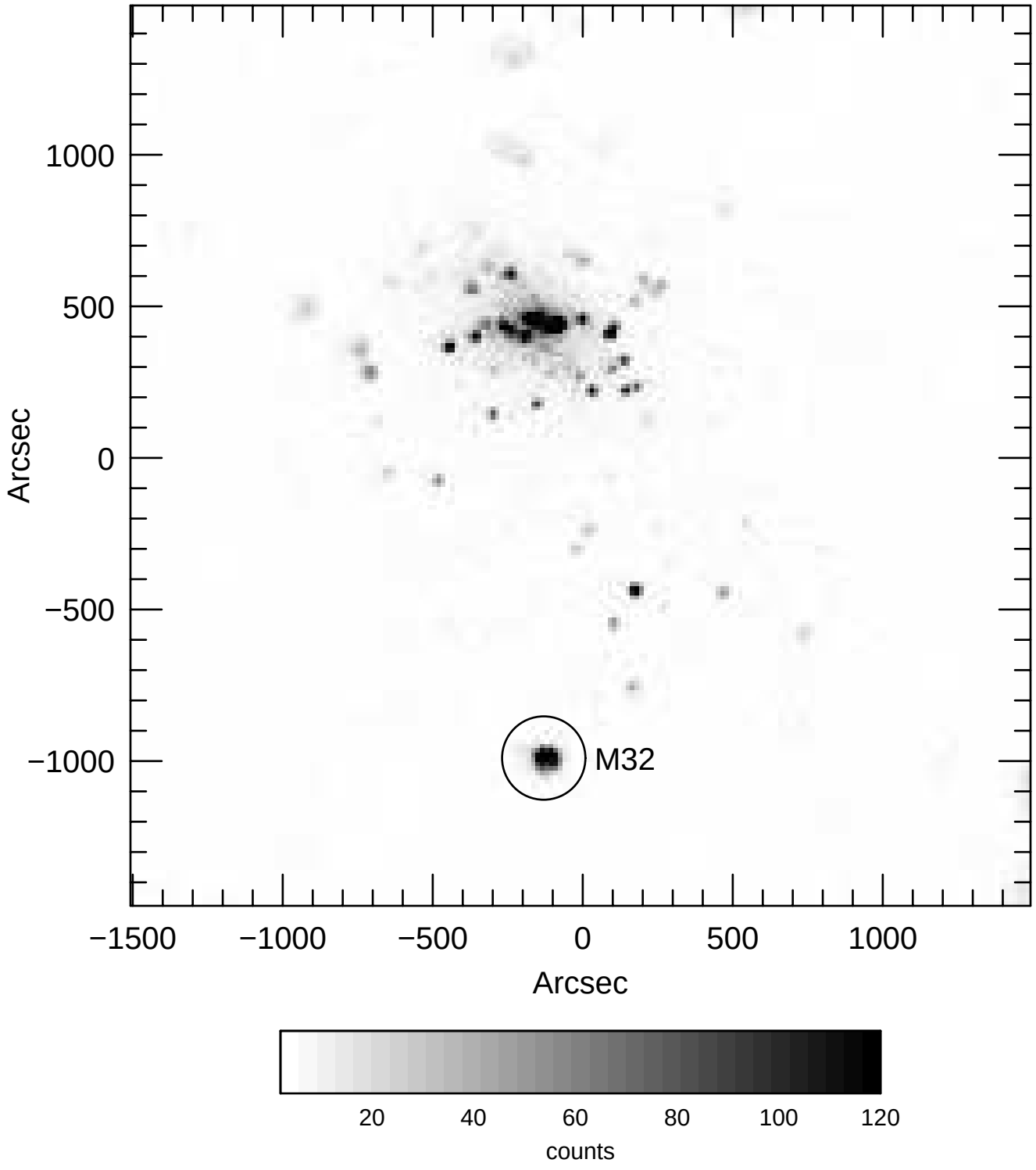

M32 Figure 2b

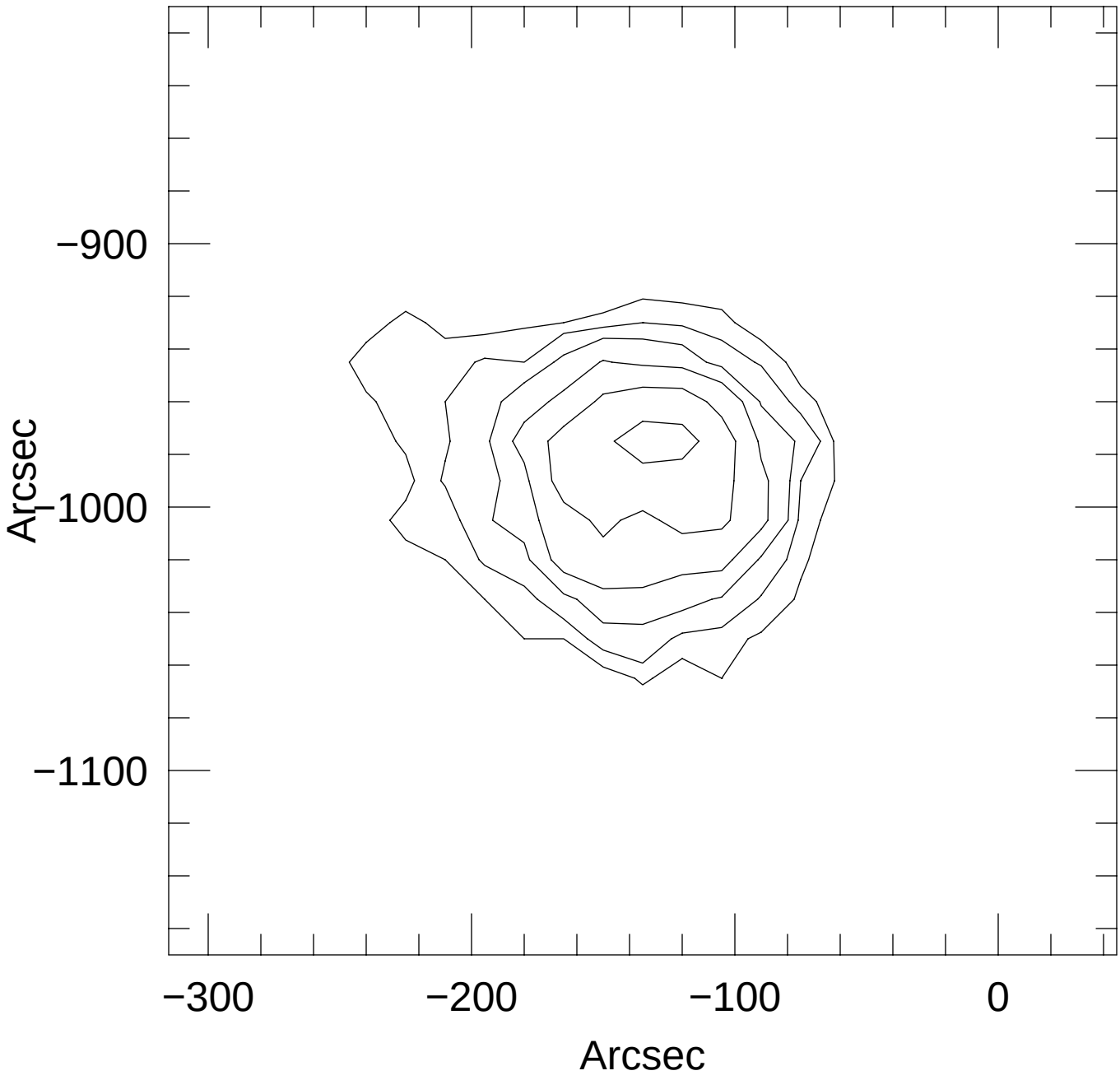

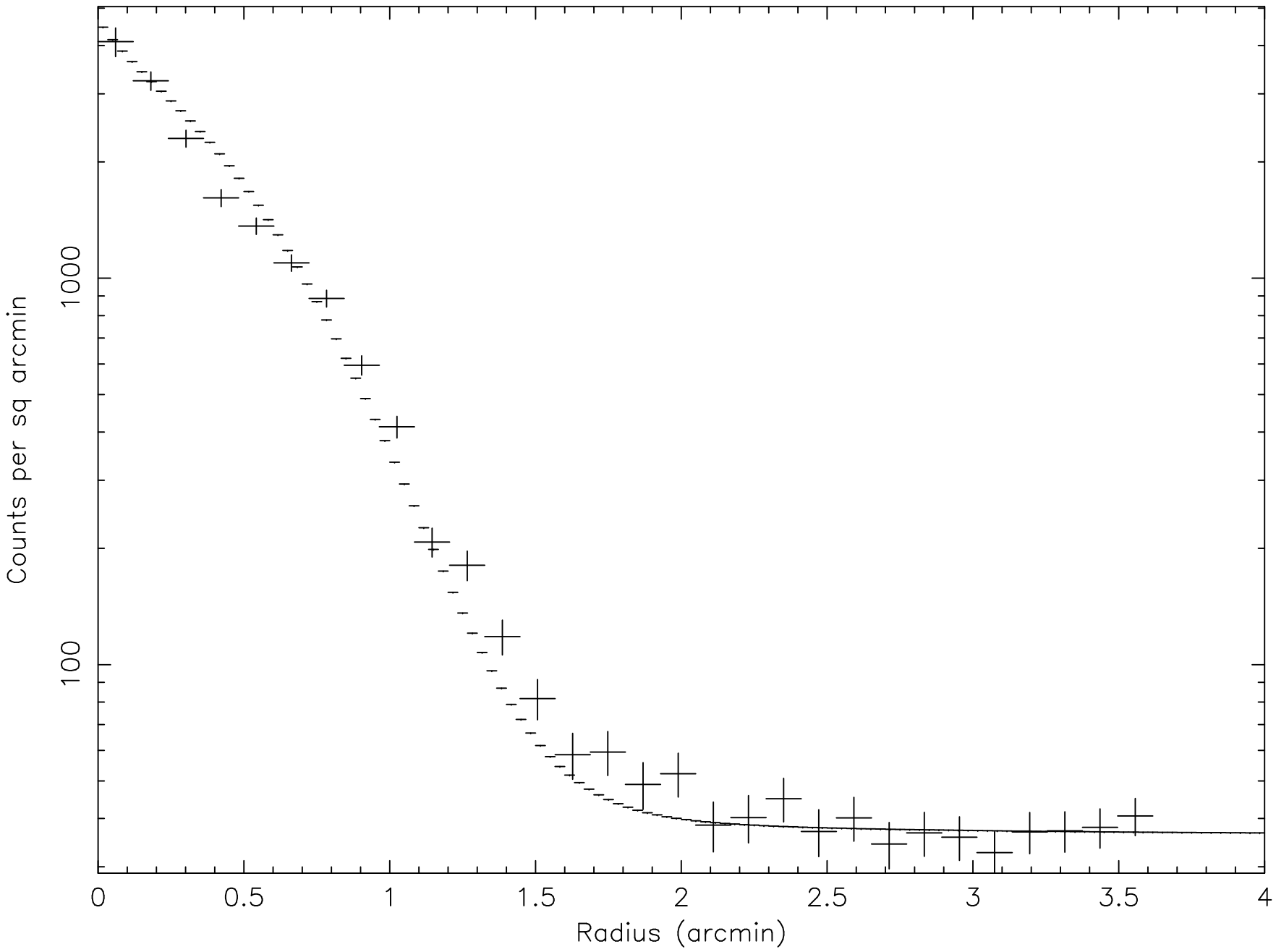
Counts per sq arcmin
1000
100
0
0.5
1
1.5
2
2.5
3
3.5
4
Radius (arcmin)

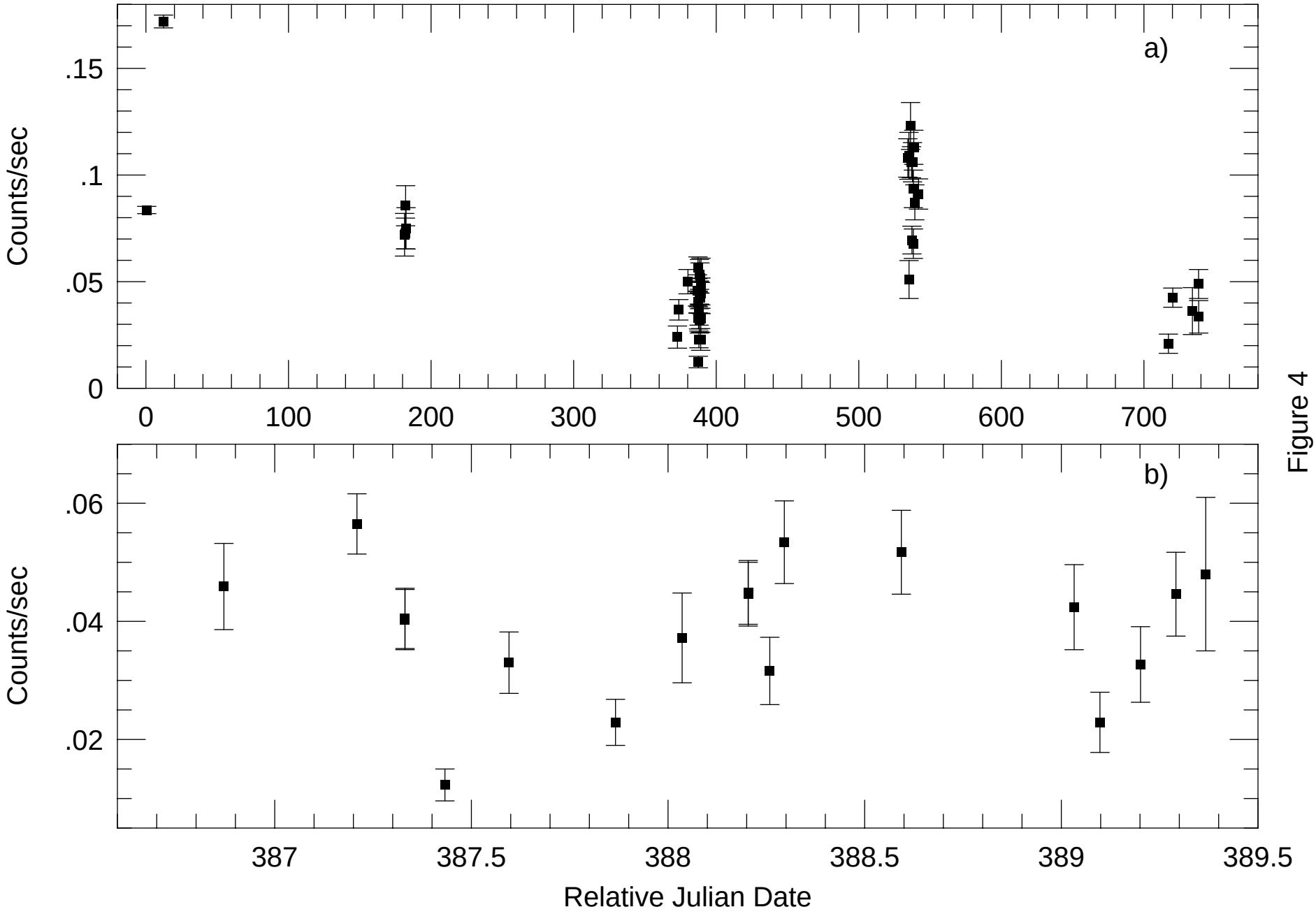
a)
b)
Counts/sec
Counts/sec
.15
.1
.05
0
.06
.04
.02
0
100
200
300
400
500
600
700
387
387.5
388
388.5
389
389.5
Relative Julian Date

Figure 4